Environmental Earth Sciences (2019) 78:499
https://doi.org/10.1007/s12665-019-8517-4

ORIGINAL ARTICLE

Differential interferometry, structural lineaments and terrain deformation analysis applied in Zero Zone 2016 Earthquake (Manta, Ecuador)

M. Cando-Jácome[1] · **A. Martínez-Graña**[1]

Received: 5 April 2019 / Accepted: 29 July 2019

Abstract
The earthquake of April 16, 2016 caused huge economic losses and human lives in Ground Zero of the city of Manta, Ecuador. The present study delimited the affected areas by superficial deformation and vertical displacements of the relief in this zone by means of the differential interferometry analysis (DInSAR), with the support of geophysical techniques such as electrical tomography of the subsoil and of georadar in combination with the analysis of concentration of structural lineaments-tectonic deformation, seismicity and geotechnical parameters such as soil liquefaction indexes, cutting wave velocity Vs30, among others. This combination of techniques allowed the spatial location with greater certainty of areas susceptible to seismic risk for construction and related to the soils typology of the Ecuadorian Construction Standard-NEC 2015. This proposed methodology improved forecasting mechanisms for the reduction of seismic risk based on maps of its susceptibility to the possible occurrence of an earthquake of magnitude as that of 16 April 16, 2016. Forecast that can be done to protect engineering works and to the population, especially in tectonically deformed areas.

Keywords DINSAR · Zero Zone · Ground displacement · Electrical tomography · Radargram

Introduction

The earthquake of Saturday April 16, 2016 at 6:58 p.m. (local time), of magnitude 7.8 (Mw, moment magnitude), whose hypocenter was located in front of Pedernales city (Manabí, Ecuador), at 20 km depth, was the result of displacement between two tectonic plates: the Nazca Plate (oceanic plate) that is submerged under the South American (continental plate) (EH/AA/JS 2016a).

The Ground Zero of the city of Manta, which is located in the parish of Tarqui, before the earthquake was the largest commercial and touristically developed city and it is the area where 206 people died. The commercial and touristic infrastructure was reduced to 10%. The lack of microzonation maps made it difficult to implement efficient construction plans based on current construction standards.

Until 2001, out of the 22 municipalities of the Manabi Province, only 3 had microzonation maps. Manta was one of the municipalities that did not have maps of natural hazards at management scales and, like the remaining provinces, the seismic hazards were handled with maps at a scale of 1:1,000,000 elaborated by the National Geophysical Institute and published later in the Ecuadorian Construction Standards NEC11 and NEC15 (NEC-11 2011).

The seismic hazard maps of this time, located the Manta municipality in Zone 4 with peak ground acceleration > 0.5 g and critical seismic susceptibility for construction. Additionally, the National Planning Secretariat-SENPLADES located the municipality of Manta in high susceptibility due to seismic hazard (ODEPLAN 2001). The study zone is located in the Manta municipality, environmental unit Littoral and geographically to the west of Ecuador. It is in turn the municipal seat of the municipality of Manta, bounded on the west by the Pacific Ocean; to the

Electronic supplementary material The online version of this article (https://doi.org/10.1007/s12665-019-8517-4) contains supplementary material, which is available to authorized users.

✉ A. Martínez-Graña
amgranna@usal.es

M. Cando-Jácome
id00709713@usal.es

[1] Department of Geology, Faculty of Sciences, University of Salamanca, Plaza de la Merced s/n, 37008 Salamanca, Spain

Published online: 06 August 2019

south with the Montecristi municipality; to the west with Montecristi and Jaramijó and to the north with the Pacific Ocean. From Zero Zone, the Tarqui parish is located, which suffered the biggest impact and destruction of the April 16, 2016 earthquake. The seismic hazard map of the National Geophysical Institute-IGN, regional location of Manta city and the Zero Zone are in Fig. 1.

Given the possibility of occurrence of a similar earthquake that caused economic loss around three billion dollars and more than 600 deaths throughout the area, we present a methodology to prevent these losses through the use of combined differential interferometry with opening radar synthetic—DInSAR, analysis of geological–structural lineaments-deformations of the ground (Cando-Jácome and Martínez-Graña 2018)], plus the results of geotechnical investigations that helped to locate spatially the susceptibility to this type of earthquakes in Zero Zone of Manta city.

Data and methods

The differential interferometry analysis (DINSAR), structural lineaments and terrain deformation with the support of geophysical–geotechnical methods followed the indicated processed in Fig. 2. The first processes consisted in performing a preliminary geological survey of the studied area through two subjects: regional–local seismo-tectonic framework (seismicity and peak ground acceleration—PGA) and geological–structural framework (regional geology, local geology and local geomorphology).

Regional–local seismo-tectonic framework

Ecuador is located in a subduction active margin where the Nazca Plate collides and subducts in the continental segments of the South American Plate and the North Andean block, at a velocity 6–7 cm per year (Marcaillou et al. 2016).

In this active margin, two seismic sources can be identified: (1) of subduction where moment magnitude—MW seism's higher or equal to 8 can be generated and (2) of cortical fault with seism generation at the interior of the continent with magnitudes of 6–7 Mw and macroseismic intensities of VIII–X. The seism analysis was conducted by the National Geophysical Institute, obtaining 8923 independent tectonic earthquakes of minimum magnitude completeness of 4.5 and a maximum of 8.8. Most of these earthquakes, with magnitude greater of 5 Mw have had their epicenter along the subduction slab.

In function of these seismic sources, the National Geophysical Institute has delimitated the coastal margin along the Ecuadorean tectonic trench in three structural seismogenic zones: structure South (Zone 3) corresponds to the Gulf of Guayaquil and the continental segment of Santa Elena, Guayas and El Oro. Central structure (Zone 2) is the central segment of the subduction zone, in the province of Manabí, activated on April 16, 2016 (Mw 7.8). North Structure (Zone 1) corresponds to the coastal area of the Esmeraldas Province (Chunga et al. 2018) (Fig. 3). The instrumental seismicity of 2016, determined a higher concentration of seismic lineaments than in Zone 2, due to the lack of thrust in the Nazca–South American plates border, where tectonic erosion is produced in the South American plate, which is above the Nazca Plate, resulting in a complex seismogenic

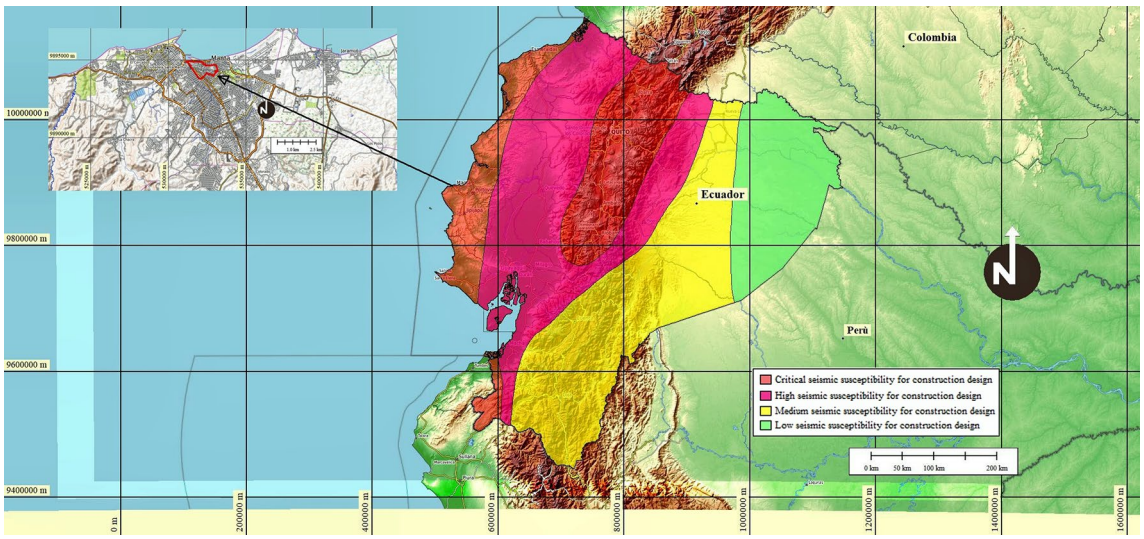

Fig. 1 2001 seismic hazard map of the National Geophysical Institute-IGN and located the Canton Manta in Zone 4 with acceleration of gravity greater than 0.5 g and degree of critical seismic susceptibility for construction design. Legend: seismic susceptibility for construction design (red: critical, pink: high, yellow: medium, green: low)

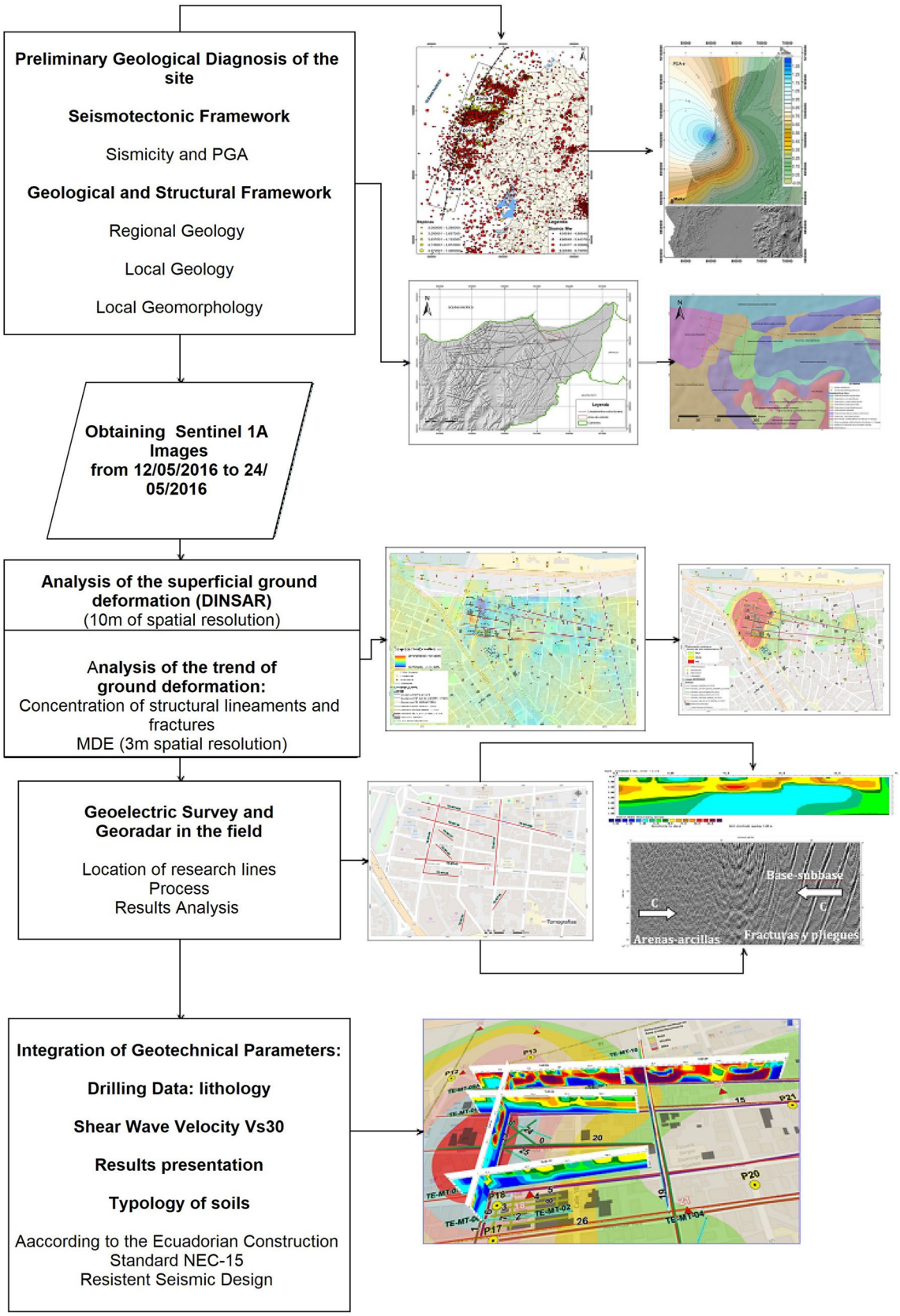

Fig. 2 Flow methodological process for the combined analysis of seismic risk susceptibility in Manta's Zero Zone

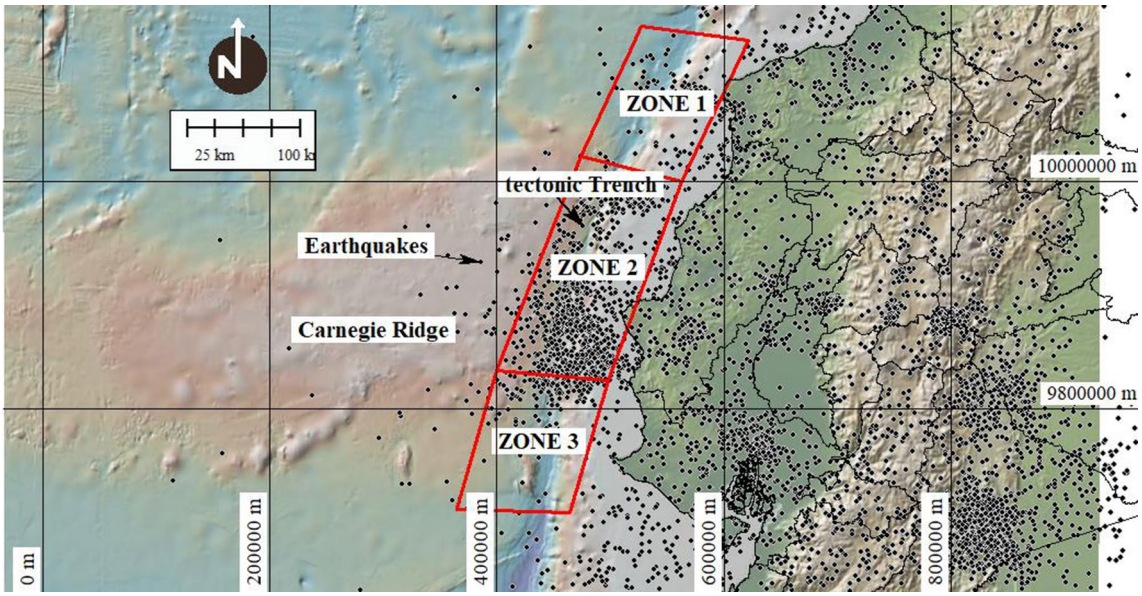

Fig. 3 Ecuador Seismogenetic Zones along the tectonic trench. (3) South Zone, Guayaquil Gulf and the continental segment of Santa Elena, Guayas and El Oro. (2) Central Zone activated on April 16, 2016 (MW 7.8). (1) Northern Zone, Esmeraldas province. Greater earthquakes concentration in Zone 2, in subduction zone due to the failure of thrust on the edge of the Nazca and Sudamericana, resulting in a complex seismogenic behavior of trust that is possibly generating large earthquakes such as that of April 16, 2016

behavior of thrust that can generate large earthquakes and surface deformations.

In the special seismic report No. 13 of April 17, 2016, the Nacional Geophysical Institute—IGN mentions that in Zone 2, higher levels of interseismic coupling (ISC), this is the reason why these segments were considered as in a process of crescent accumulation of energy, with higher probability of earthquakes occurrence (EH/AA/SV/MR 2016b). The zone where the earthquake of April 16, 2016 happened and its respective replicas coincide with the 1942 earthquake and with the norther border of the replica zone of the 1998 earthquake (Bahia de Caráquez). Historically, the subduction process originated the earthquakes of January 31, 1906 (MW 8.8), which is the largest recorded in Ecuador and the sixth largest at a global scale; and the one on May 14, 1942 (MW 7.8); January 19, 1958 (MW 7.8) and December 12, 1979 (MW 8.1). The closer cortical geological faults to Manda are the Barbasquillo-NE fault, located in the Northeast, at a distance of 4 km from Zero Zone, estimating a maximum magnitude of 6.3° and a PGA value of 0.33 g, and the Aromo Norte fault localized between 2 and 3 km of Zero Zone, faults that can possibly generate earthquakes about 6.8 MW and a PGA of 0.30 g.

Seismicity and PGA

The distribution of the regional deformation Jama-Pedernales, according to the PGA (m/s^2) has resulted in Manta city having high seismicity levels with ground acceleration factor of 0.35–0.55 g. These values related with the seismicity of the central segment (Zone 2). The population at 55 km of this deformation is very susceptible to being affected by the active seismicity of the mentioned deformation (Fig. 4a).

In Zero Zone, these seismogenic structures were possibly responsible for the earthquake of April 16, 2016 and the following aftershocks due to the subduction process and the displacement of the Carnegie Mountain Ridge under the continental zone in Central Zone 2 in front of the coastline of the Manabí Province (Gutscher et al. 1999). As a consequence, these earthquakes destroyed the engineered infrastructure with loss of human life. The silty, clayey and sandy soils underwent liquefaction processes with very shallow water levels in depths of 2 m which fractured by the displacement, possibly by compression and dilatation (Fig. 4b).

Regional and structural geology

Regionally, Manta municipality is located in a tectonic deformation in the Barbasquillo and El Aromo fault systems. Displacement faults headed in NE–SW and E–O directions go through the Coast Mountain Range with the presence of minor faults that appear from San Lorenzo, San Mateo Manta until Jaramijó.

This tectonic deformation is in the occidental margin of the Ecuadorean Pacific Ocean, between the borders of Colombia and Peru, very close to the Ecuadorian trench, directly in front of the Carnegie Mountain Ridge, oceanic mountain with a height of 2 km created from the same

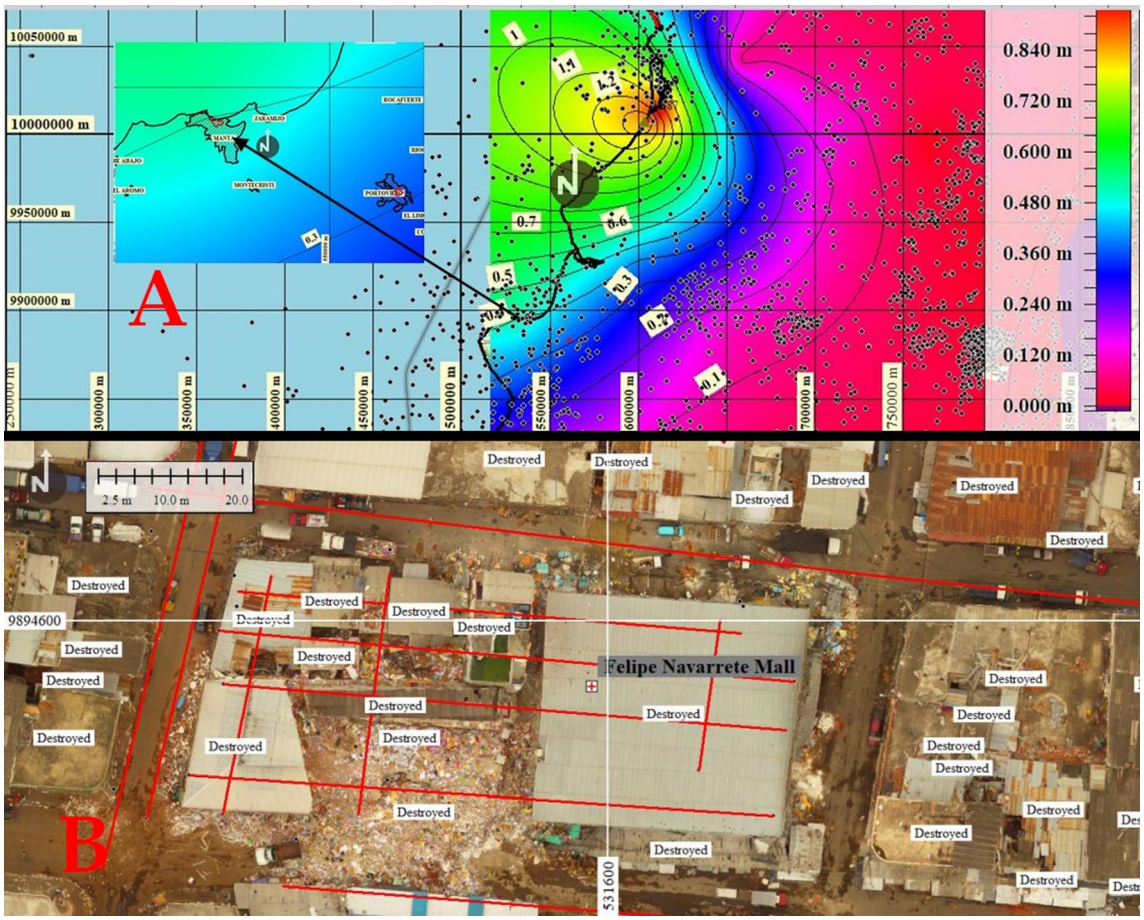

Fig. 4 Up: The regional map of isosista of PGA is observed, from the Jama-Pedernales regional deformation and its distribution, according to the data obtained of accelerograms of the IG-EPN, with visualization of maximum values of amplitude (m/s^2). In detail, the distribution of the PGA (m/s^2), in Manta city with high levels of seismicity and soil acceleration values between 0.35 and 0.55 g. Values related to the seismicity of the central segment (Zone 2). Down: Deformation of the soil in clay, silty and sandy soils on which houses and streets have collapsed in Zero Zone. Down center. Aerial view with drone of the destruction of a building.

hotspot which originated the Galapagos Island (Norton 2010). The coastline is located in the intern wall of the Ecuadorian Oceanic Trench, which is the main oceanic character in the Subduction Ecuadorian system. This is a dual Arc–Trench system of high complexity that represents the boundary between two cortical plates moving in opposed directions. In this case, the Nazca oceanic plate is moving to the East, while the South American continental plate is moving to the West. As result of this confrontation, the surface deformation of the Barbasquillo and El Aromo faults can be evidenced in Fig. 5a. In the area of study, structural lineaments that are controlling the drainage patterns in the coastal margin and have relation to the regional fault systems of great influence in the relief deformations as well as in civilian structures that settle on them. These geological lineaments in the Zero Zone, are directly related with the regional geological fault Barbasquillo-NE and move mainly in the E–W, NW–SE and NE–SW directions (Fig. 5b).

Lithology and local geomorphology

Information from Geotechnical investigation of Geosuelos S.A. and Geophysics obtained from the Secretariat of Risk Management (Tomography's and radargrams) has confirmed that the lithology in the municipality of Manta is made up of Quaternary sedimentary deposits, among these, modern alluviums of the Canoa Formation and deposits of the Tablazo Formation (Fig. 6a). The lithological materials in the Canoa Formation (Pc) are silty sands with the presence of clays, thin yellow sands, slightly compact sands and medium to coarse grains of gray color. Modern alluviums (Qt) of detrital material are transported and deposited as sand, gravel, clay and silt. The Tablazo Formation (Qt), which is areas in a process of elevation, is composed of three facies. The Tablazo Alto attributed to the Lower Pleistocene contains lumaquelas and calcareous sandstones, deposited on open beaches. The Tablazo

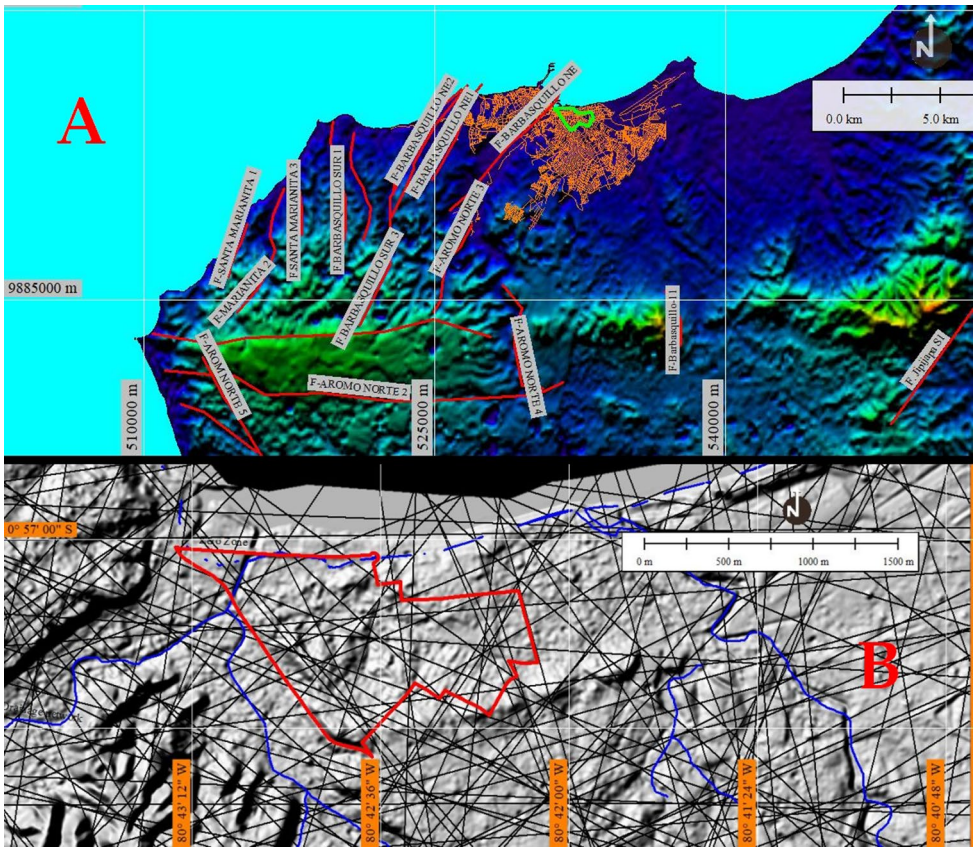

Fig. 5 **a** The shock of the Nazca and South American continental plates has deformed the earth's surface with the occurrence of the Barbasquillo and El Aromo fault systems that generate large earthquakes and deformations of the earth's surface as happened on April 16, 2016. **b** Concentration of geological lineaments in Zero Zone and nearby areas

Medio contains fossils that suggest a brackish facies and the Tablazo Bajo that corresponds to an open sea of the Upper Pleistocene. The peninsula of Manta is presented as a structure with East–West orientation, from the Cape of San Lorenzo to the Hill of Montecristi. The Dome or highest geoforms extend from El Aromo, with a height of 365 m, to Montecristi with 600 m. In Ground Zero there are different sedimentary facies, such as recent beach sand, sand barrier coastal, sand, sandy loam in tidal flats and sandy loam facies in soils of colluvial origin.

The regional units of the littoral landscape which dominate this sector correspond low hilly reliefs to mean reliefs with eroded springs on siltstones, clays and sands; Surfaces of surrounding mesas and abrupt panels on sandstones, conglomerates, lumachelles and sands; relief hills high to very High over volcanic rocks and ancient sedimentary volcanic; Quaternary sedimentary deposits, among these, modern alluviums of the Canoa Formation and deposits of the Tablazo Formation (Winckel 1997). The soils of the region are mainly clayey. The relief shapes present in the Manta municipality have their origin in the tectonic–erosive processed (mesas, very low, low, medium and high hilly reliefs), structural (chevron surfaces), denudative (ancient and recent colluviums, recent colluvium–alluvials, medium and low terraces and causes of rivers, fluvial valleys and cliffs) and depositional (marine tables, canyons, ancient and recent colluviums, coastal plains, littoral spits and beaches). The geomorphology of Zero Zone presents coastal and fluvio-marine sedimentary reliefs of depositional genesis, with geomorphological units well marked such as marine mesas in extensive terraces composed by very fine-grained sands, gravel, silt and clays, on very low slopes (Fig. 6b).

Terrain deformation analysis by differential interferometric synthetic aperture radar-DINSAR and structural lineaments

The following process consisted in performing a deformation analysis of the terrain through the differential interferometric synthetic aperture radar-DINSAR technique to determine sinking zones, subsidence, and terrain inversion and analyze the tendency of these surface deformations possibly generates by surface Rayleigh waves associated to concentration of structural lineaments extracted from a digital elevation model with a spatial resolution of 4 m. This process can be evidenced in Fig. 7.

Finally, this information was integrated with the results of the geotechnical and geophysical studies in order to define the typology of the soil in Zero Zone and its bearing capacity for construction according to the Ecuadorian Construction Norm NEC-15. The DINSAR analysis was elaborated based on two SAR SENTINEL images 1A of a

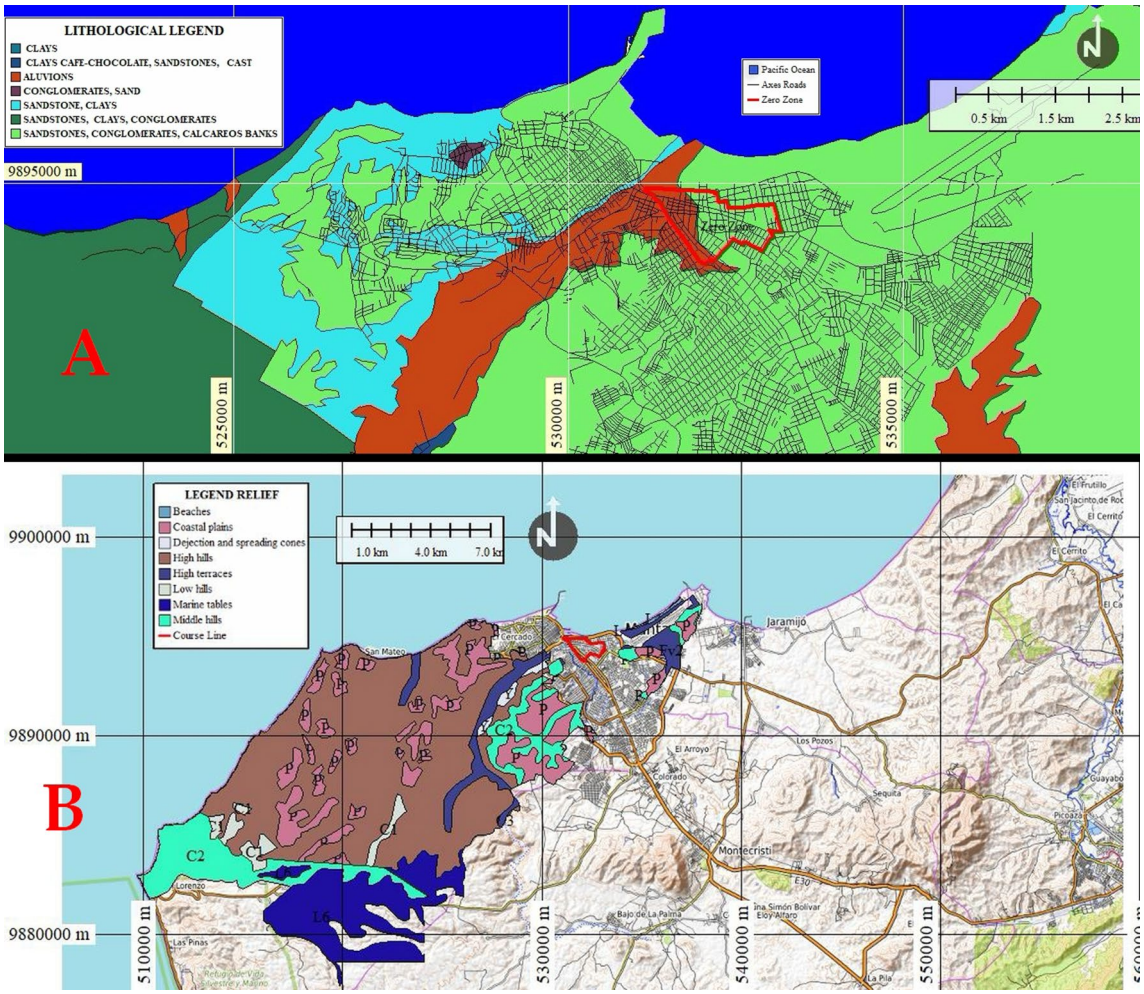

Fig. 6 **a** Local lithology in Zero Zone of Tarqui, is conformed by Quaternary sedimentary deposits, among these, modern alluviums of the Canoa formation and deposits of the Tablazo formation. **b** The Zero Zone geomorphology present coastal sedimentary and fluvial marine reliefs of depositional genesis, with morphological units well marked as surfaces of marine tables in extensive marine terraces composed of very fine grained sands, gravel, silt and clays, in very low slope

spatial resolution of 18 m, the SLC processing level (single look complex), an image of April 12, 2016 before the earthquake and another image of April 24, 2016 after de earthquake (IASR 2016a). The terrain deformations (sinking and lifting), were obtained through the SARScape module of ENVI software.

The steps taken to obtain the terrain sinking and lifting map by DINSAR interferometry were the following ones: (1) generation of the interferogram, apply an adaptation and generation filter; unroll phase, tuning and applanation phase (correction of orbit inaccuracies), height conversion and geocoding phase and displacement and geocoding phase. (2) The final product was obtaining an image of vertical displacement of the land after the earthquake (Fig. 8a). The analysis of the concentration of the structural lineaments was obtained from the application of Hydrological Model D8 (Cando-Jácome and Martínez-Graña 2018) (Fig. 8b).

Tomographies and georadar survey in the field

Depending on the zones of deformation of the terrain found in Zero Zone, taking the one with the bigger deformation and delimited by the Felipe Navarrete Mall, Banco del Pichincha and Central Market, the geophysical investigation network was delimited, electric tomography and georadar studies to carry out the subsoil investigation. In the same electric tomography traces, georadar techniques were applied to get coherence with the resistivity and conductivity results. This network is seen in Fig. 9. The combination of electrical and georadar tomography techniques has been applied in order to find deep objects with lower resolution and shallow objects with higher resolution, respectively. This combination was correlated with the geotechnical results obtained from Geoestudios S.A. (Antón and Avilés 2017), which improved the diagnosis of the equilibrium state of the subsoil.

Acquisition of Sentinel 1A images

Analysis of subsidence and subsidence based on interferogram values DINSAR

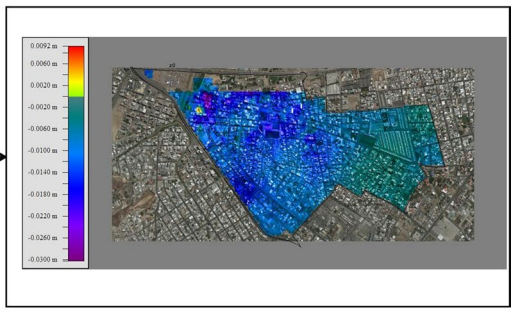

Spatial determination of the zones of surface deformation using the subsidence-subsidence values and structural lineaments obtained from the digital model of elevations of 4 m of spatial resolution.

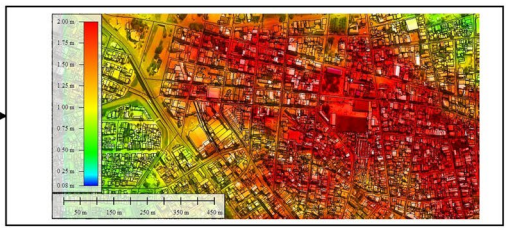

Integration of the results of the interferometry by DINSAR and of the terrain deformation traces

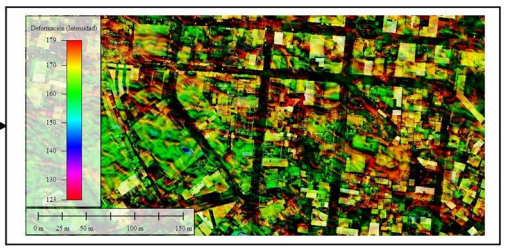

Spacial designation of geophysical research lines in the zones of maximum deformation of the terrain, geo-electric and georadar in the field

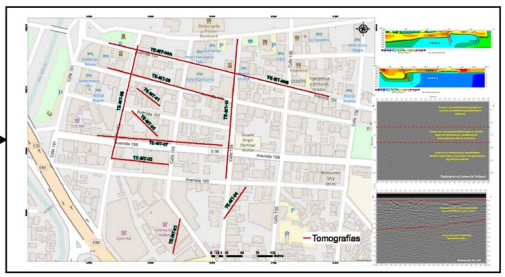

Corelation with cutting speeds Vs30, and lithology obtained from perforations: b electrical resistivity-electrical conductivity-cutting speed Vs30-lithology-soils.

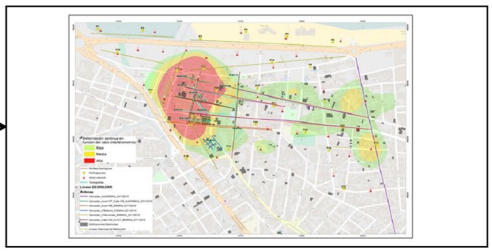

Determination of soil types for earthquake-resistant design in relation to the current Ecuadorian Construction Standard NEC-15.

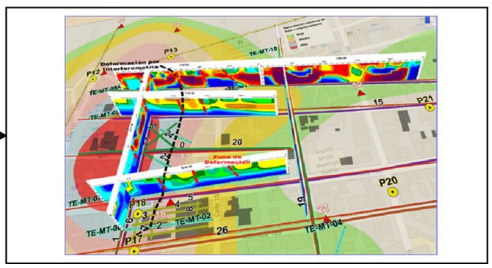

◂**Fig. 7** Flow of the process applied in the terrain deformation analysis using the Differential Interferometric Synthetic Aperture Radar-DINSAR technique to determine subsidence, inversion of the relief zones and find the trend of these superficial deformations associated with tectonic traces possibly generated by waves superficial Rayleigh and Love, using a digital model of elevations of 3 m of spatial resolution of the affected areas due to the earthquake and integration of geotechnical field data

Electric tomography

Is a non-destructive geophysical technique used for subsoil study, which consists of introducing a voltage of continuous electrical current in the surface of the terrain through two electrodes that is measured by another pair of electrodes? From the obtained value of injected electrical current and the received voltage in response of the lithological materials

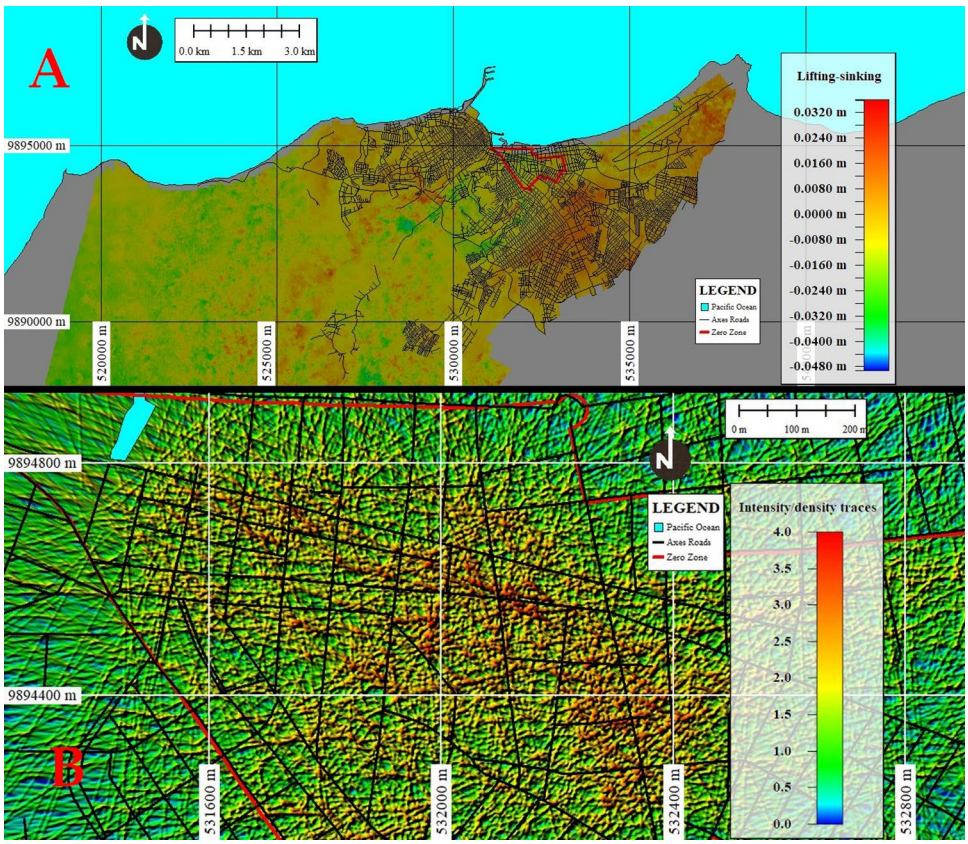

Fig. 8 **a** The deformations of the terrain (subsidence and uplift), were obtained from the processing of two images after and before the earthquake of April 16, 2016. The deformations cover ranges of 4 cm up to 8 cm of regional subsidence. **b** Zero Zone. Local maximum deformation trend obtained from the concentration of structural lineaments and fractures extracted from the Digital Model of Elevations of 4 m of spatial resolution

Fig. 9 Location of the network of geophysical research lines, electrical tomography and georadar in the areas of maximum deformation of the ground, for the investigation of the subsoil. In the same line of electrical tomography, the georadar was applied to obtain coherence in the resistivity and conductivity responses

through which it crosses, the "apparent resistivity" of the subsoil is obtained which the difficulty is found by the electric current when it crossed a determined material. Electric resistivity is a specific property of each material (it does not depend on its geometric characteristics), it is measured in ohm meters (Ω m), and it is inverse to the electric conductivity (Toprak et al. 1999; IASR 2016b; Vidal Montes et al. 2016; Antón and Avilés 2017). Each type of material presents a "real" resistivity range more or less characteristic/more or less characteristic. Empty cavities (filled with air) have an apparent resistivity that tends to infinity. Terrains saturated with saline solutions are higher conductive, thus having low resistivity. Most of the rock and soil components are considered as low conductive materials or with a high resistivity, excepting some cases such as some metallic minerals. The measurement consists in determining the resistivity distribution from a number of measurements made from the terrain surface with electrodes that are "nailed" in said surface. In this study, in accordance with the coastal sedimentary environment of the land, the gradient Schlumberger device was used with an electrode spacing from 1 to 5 m, with longitudes of 40–200 m and depths from 7 to 37 m. Eleven electrical tomography lines were erected in the areas of maximum deformation of the terrain, mainly in the Navarrete shopping center and nearby areas.

For the migration and inversion process of the field measured apparent resistivity, the finite differences method was used which generated a trustworthy interpretation method. Local optimization of the resistivity values with a vertical filter was used due to the nature of the subsoil (sedimentary layers), decreased damping of the signal in depth and the resistivity ranges for all sections were standardized (Fig. 10a).

Georadar

In the same maximum deformation zone, the georadar technique was applied (ground penetrating radar—GPR), which is a non-destructive geophysical method used for the exploration of the subsoil from the surface, through the emission and reception of electromagnetic waves, which vary in function of the electromagnetic properties of the material, as well as some parameters of the surrounding environment. The variations in the electromagnetic waves are caught by the receptor and later, sent to a registry unit where the data are processed in order to produce a high-resolution image (radargram). The deepness of the investigation, as well as the resolution depended on the type of the employed antenna

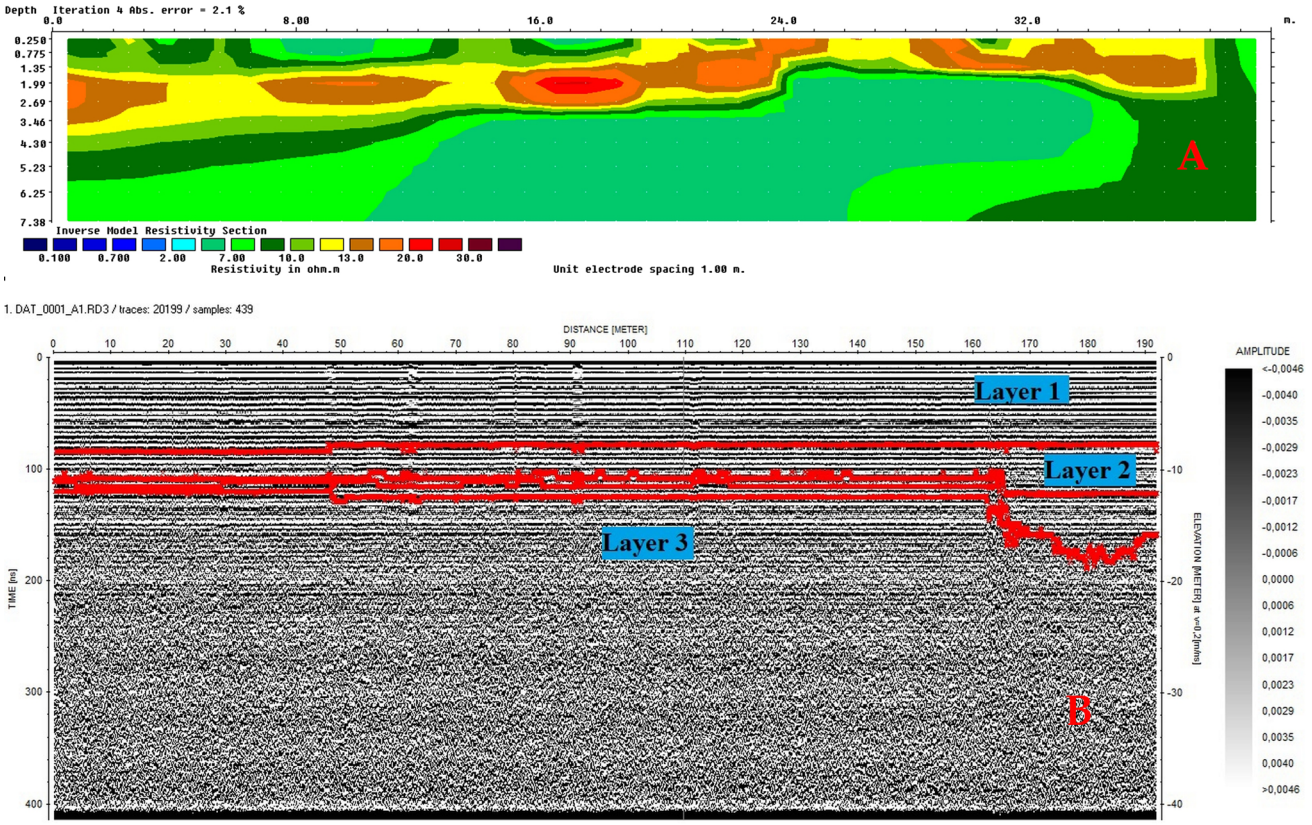

Fig. 10 **a** Migration and inversion of the apparent resistivity measured in the field done using the finite difference method, which generated a reliable model interpreted. Final radargram. The processing of the data was done with the Reflexw software with the following steps: **b** Elimination of zero time, background removal and linear gain smoothing applied

that in this case were Mala Proex armored antennas of 250 (with a depth of investigation of 30 m) and 800 MHz (depth of 2 m). The higher frequency antennas get higher resolution radargram, but with lower depth of investigation. Most of the rocks and subsoils in which the studies are carried out can be considered as insulators. In these mediums, the electrical conductivity exists due to the presence of saline flow in pores and fissures. It means that the greater the content of water and dissolved salts and the porosity of the medium, the greater its conductivity. The unit of measurement is Siemens/meters (S/m) and is the opposite of resistivity.

The data were processed with Reflex software from a raw image (Fig. 10b). Subsequently, a pass band filter was applied to eliminate the noise and highlight the signals that can represent an underground object. Zero time was eliminated to define the reference zero of the image, for the case of the definition of strata; it will be the current surface of the land to eliminate the environmental noise. Finally, a linear gain and gain filter were applied to improve the visualization of objects in the subsoil. Once obtained the electric tomographies and radargrams within the maximum continuous deformation areas in the Zero Zone, the resistivity and conductivity, were correlated with the obtained values from the geotechnical–geophysical information of Geosuelos S.A., and their spatial correlations were analyzed in the distribution of the types of soils for the seismic design.

Results

The electric tomography and radargrams were related with resistivity factors, lithological values of 17 perforations (compactness–rigidity), SPT testing (liquefaction, shear stress, subsurface conditions), CPT (resistance and elasticity of its soil–subsoil), surface wave analysis tests in multichannel-MASW arrays and microtrepidation analysis in multichannel-MAM arrays to find cutting speeds Vs30 (Antón and Avilés 2017) (Fig. 11).

Tomography and radargram

In general, in Zero Zone of Tarqui, relatively low resistivity values were found (0.3–60 Ω m), which reflect the nature of the subsoil, the same which is constituted by unconsolidated sands, silty sands and silty–sandy loams. Those behave like soft to semi-rigid soils that, at the study site due to the earthquake of April 16, 2016, liquefied and were conditioning factors for the collapse of the buildings that were built without standardized construction procedures. The majority of soils in Zero Zone are found within the ML groups (low plasticity inorganic silts), MH (inorganic silt mud, clay and fine sand mixture) and CH (elastic expansive clays).

During the earthquake, many civil structures in Zero Zone suffered subsidence and displacement. In the superior horizons of up to a depth of 5 m, the pavements of reinforced concrete and asphalt were deformed in its entirety. At greater depth, an area of very low resistivity was found, probably because the sandy sediments are currently saturated with water due to the presence of high water tables. The main lines of tomographies and radargrams of the subsoil obtained in Zero Zone of Tarqui are summarized below.

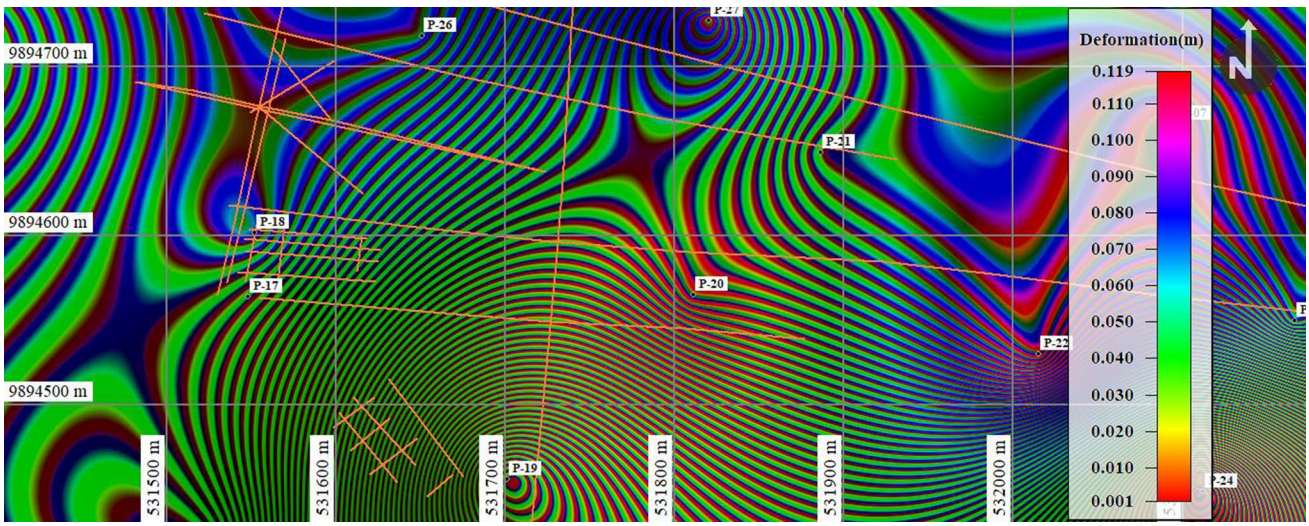

Fig. 11 Dinsar-Density deformations and distribution of electrical tomographies, georadar lines (orange color), points of perforations and values of REMI + MASW with the objective of classifying the terrain for seismic design (cutting speed Vs30) within the areas of maximum continuous deformation of the Zero Zone in Cental Market and the Felipe Navarrete Mall P17 and P18 points

Electrical tomography TE-MT-01 and radargram between 102 street and Av. 107, corner

Tomography length: 40 m. Depth of penetration: 12 m. Result: three subhorizontal layers with resistivities between 6.29 and 15.96 Ω m with an average of 9.35 Ω m. Radargram antenna: 250 MHz with length of 35 m and depth of penetration up to 30 m. *Interpretation*: the first surface layer corresponds to soft sandy–silty soils with a thickness of 1 m. A second semi-rigid layer composed of poorly classified sands that have a thickness of 5 m. In this layer in the position $L = 24$ m, a change in thickness was evidenced, which suggests the presence of a zone of significant deformation. Under this layer, an area of low resistivity was determined. In the radargram, 0–8 m depth corresponds to very homogeneous and poorly consolidated soils, as indicated by the response of Vs30. From 8 to 12 m there are little conductive soils with a high degree of deformation. After 12 m again, there are consolidated soils that present a medium-to-low conductivity.

Electrical tomography TE-MT-02 and radargram between 102 street between Av. 108 and 109. Felipe Navarrete Mall, Pichincha Bank and Central Market. Zone of maximum ground deformation

Tomography Length: 90 m. Depth of penetration: 18 m. Result: a horizontal surface layer of 3 m depth, with moderately high resistivities between 3.54 and 19.83 Ω m, with an average of 7.70 Ω m. Radargram antenna: 800 MHz. In the radargram, it was observed that from 0 to 30 cm pavement is located and from 30 cm to 50 cm begins the asphalt folder with concrete reinforcement which is deformed and fractured. Below the 50 cm to 100 cm, there are sediment horizons a little more consolidated. However, there are zones or "windows" that were intensely deformed, possibly due to the earthquake of April 16, 2016. Interpretation: semirigid sandy-silty soil. In this layer, there was an abrupt change in thickness that suggests the presence of a zone of significant deformation. Under this layer, an area of low resistivity was determined. Along this block were the Felipe Navarrete Shopping Center, Banco de Pichincha and the Central Market that totally collapsed with the largest number of human victims (96). From the 100 cm, marine sediments possibly of marine transgression deformed in contact with the superficial parts of the subbase and base of the deformed path are observed. This line can be correlated with the previous radargram (102 Street and Av. 107), which also showed maximum deformations of the terrain. This zone is the one of greater deformation obtained by interferometry and numerical modeling of structural lineaments and superficial deformations of the terrain based on the analysis of concentration of structural lineaments.

Electrical tomography TE-MT-03 and radargram in Velboni commercial

Tomography length: 65 m. Depth: 12.5 m. Results: a horizontal surface layer that reaches up to 5 m deep, with moderately high resistivities between 4.06 and 31.43 Ω m with an average of 11.62 Ω m. Radargram antenna: 250 MHz, with a length of 44 m and penetration depth of 30 m. Interpretation: semi-rigid sand–silty. Underlying an area of low resistivity was found. No areas of significant deformation were found. (C) In the radargram, 0–8 m depth corresponds to highly homogeneous conductive soils and a few consolidated (possibly filled) as indicated by the response of Vs30. From 8 to 15 m there are soils with a medium conductivity and high deformation degree, possibly caused by coseismic effect. After 15 m again, highly conductive and consolidated soils appear, possibly as a response to transgressions and marine regressions.

Electrical tomography TE-MT-04 and radargram between 104th street and Av. 109

Tomography length: 55 m. Depth: 11 m. Results: a horizontal surface layer of 4 m depth, with moderately high resistivities between 1.74 and 44.13 Ω m with an average of 10.29 Ω m. Interpretation: semi-rigid silty sands. Interpretation: Underlying an area of low resistivity was found. There are no significant deformation zones along the studied line, except for a slight thickness reduction anomaly between the positions $L = 16$ and $L = 37$. Radargram antenna: 250 MHz, with a length of 192 m and depth of penetration of 30 m, it was determined that from 0 to 10 m depth correspond to highly conductive soils homogeneous and few consolidated (possibly filled) as indicated by the answer of the Vs30. From 8 m to 17 m deep, there are soils with a medium conductivity and with a high degree of deformation as observed in the distances from 40 to 60 m, 75 to 85 m, 110 to 113 m, and 170 to 172 m, possibly caused by coseismic effects. From the depth of 17 m depth, highly conductive and consolidated soils are again present, possibly as a response to continuous episodes of marine transgression and regression. The images of the tomographies and radargrams: TE-EM-01, TE-EM-02, TE-EM-03 and TE-EM-04 can be seen in Online Appendix A.

The DINSAR interferometry methodology corroborated the existence of deformations of the ground surface in the

Zero Zone obtained through the analysis of the concentration of structural lineaments. Both mechanisms coincided in the geographical delimitation of the area of greatest deformation, the Felipe Navarrete Mall, the Banco del Pichincha and the Central Market, site where more than 96 people died due to the earthquake. The deformation zones determined in the subsoil based on electrical tomographies and radargrams are aligned following the superficial tendency of the deformation determined by the interferometric analysis and density analysis of structural lineaments.

It is concluded that in general, soils from 0 to 5 m deep are highly conductive, soft, with cutting speeds of 50–115 m/s, which corresponds to sandy soils on poorly consolidated sand–silt strata present in the maximum deformation zone. Within the classification of the soil typology of NEC 2015, the zone falls in categories E and F (unconsolidated fillings) of very bad seismic response. Outside the zone of maximum deformation are semi-rigid soils that correspond to type D soils (between 7 and 14 m deep). The MAM + MASW tests carried out by the company GEOESTUDIOS SA confirmed the results obtained by the geophysical analysis, so it can be stated that in the study area there are Type D, E and F soils according to the NEC-2015, with values of Vs30 between 50 and 360 m/s. The aforementioned results allowed differentiating three types of soil profiles for the seismic design in Zero Zone of Tarqui.

Profile 1 Consisting of 2 differentiable layers: the first layer from the surface to 7 m deep with Vs = 50 m/s at Vs = 150 m/s. The second layer reaches up to 30 m deep with Vs = 200 m/s at Vs = 300 m/s.

Profile 2 Constituted by 3 differentiable layers: the first layer from the surface to 5 m depth with Vs = 100 m/s at Vs = 160 m/s. The second layer reaches up to 10 m deep with Vs = 160 m/s at Vs = 200 m/s. A third layer reaches up to 30 m deep with Vs = 210 m/s at Vs = 350 m/s.

Profile 3 Consisting of 3 differentiable layers: the first layer from the surface to 7 m deep with Vs = 110 m/s at Vs = 155 m/s. The second layer reaches up to 15 m deep with Vs = 180 m/s at Vs = 250 m/s.

A third layer reaches up to 30 m depth with Vs = 230 m/s at Vs = 393 m/s.

The result of the analysis of the local deformation tendency allowed observing the concentration of the deformations that arose in the study area and its continuity. The greatest concentration of deformations was observed between streets 101 and 104 and avenues from 105 to 109 of the Tarqui zone, where the Felipe Navarrete Mall, the Banco del Pichincha and the Central Market were located, and the same ones that collapsed in its whole. The coincidence between the destroyed infrastructure and the concentration of structural lineaments can be seen in Fig. 12a.

Discussion and conclusions

The Felipe Navarrete Mall and its surroundings can be seen in Fig. 12a; it is the area of maximum deformation determined in the subsoil and based on electrical tomographies and radargrams. This zone is aligned following the superficial tendency of the deformation obtained with the interferometric analysis and concentration of structural lineaments (Fig. 12b). This deformation of the topographic relief coincided with the geotechnical results obtained by Geosuelos S.A. in the Lateral Displacement Index—LDI that at Ground Zero caused lateral displacements due to liquefaction in the subsoil, appearing on the surface cracks, fractures and sand volcanoes plus the displacements and settlements of the structures (Martínez-Graña et al. 2013; Montes et al. 2017) (Fig. 12c). The Felipe Navarrete Mall and its surroundings are in a place of maximum ground deformation,

The intense soil deformation, the high conductivity values, the liquefaction and the low-resistivity cutting wave velocity Vs30 implied that, from the geological point of view, alluvial soils and young beaches are saturated and have greater susceptibility to erode due to its more liquid than solid behavior. This behavior is an indicator of the liquefaction potential caused by the earthquake and is the one that has caused the intense and severe damage to the foundations of engineering structures.

The DINSAR interferometry methodology, based on the Sentinel 1A images, without cost, corroborated the existence of deformations of the ground surface obtained from the analysis of the concentration of structural lineaments in the Zero Zone. Both mechanisms coincided in the geographic delimitation of the area of greatest deformation where the Felipe Navarrete Shopping Center, the Pichincha Bank and the Central Market were built, a site where more than 96 people died due to the earthquake ground shaking.

The correlation of the geotechnical–geophysical parameters such as the average shear wave velocity of the upper 30 m–Vs30, lithological records, liquefaction indexes, geophysics such as resistivity, conductivity and the intensity of the topographic deformation allowed to analyze the response of the site to predict its geotechnical capacity due to the soil vibration caused by the earthquake of April 16, 2016. This predictive capacity could have been obtained years before the earthquake occurred based on the deformation of the relief.

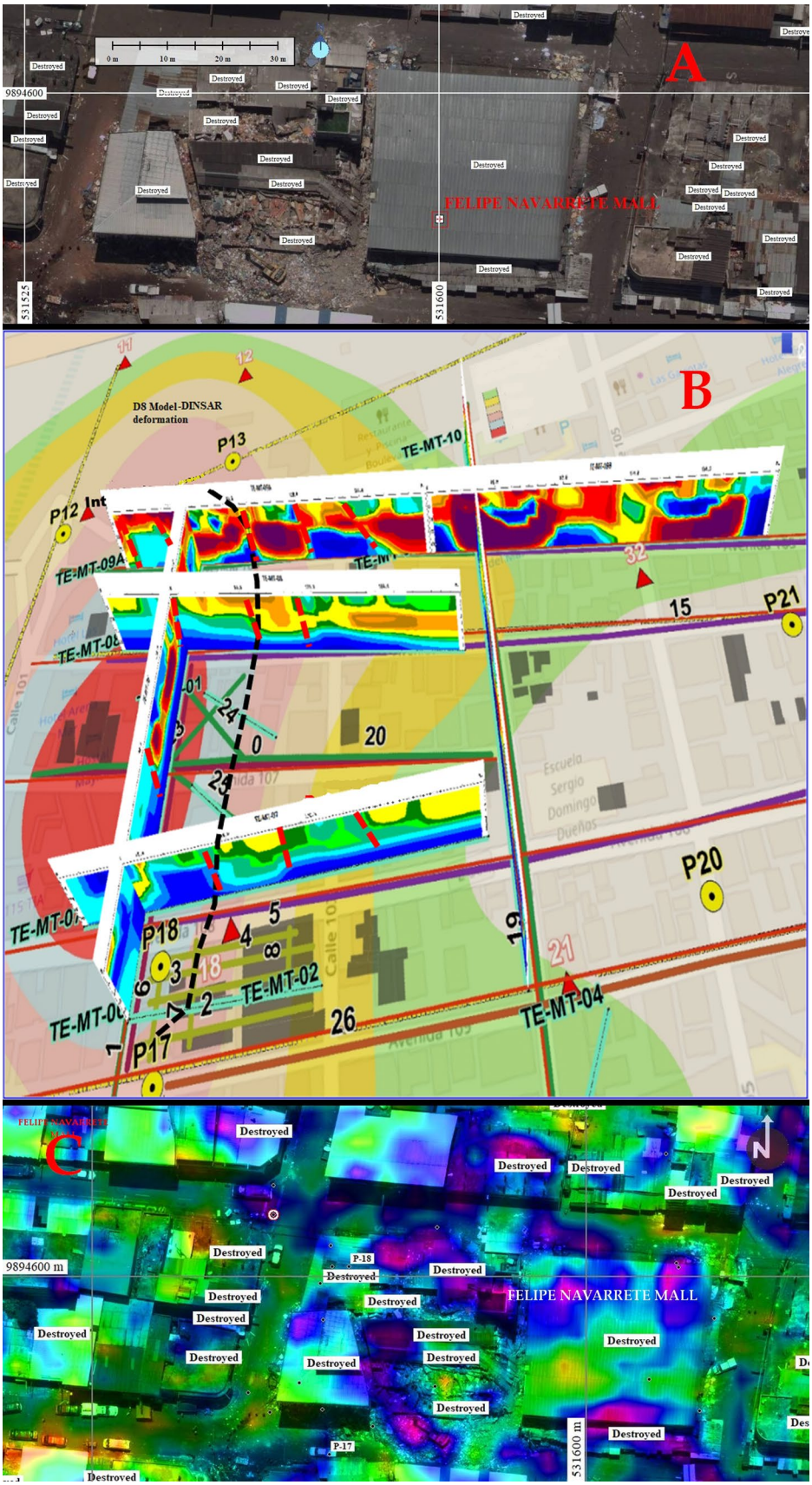

Fig. 12 **a** Location of the F. Navarrete Mall, Banco Pichincha, Central Market and nearby sites and nearby places. **b** Maximum deformation obtained from the interrelation of the DINSAR method and guidelines and density of structural lineaments. **c** Concentration of fractures analyzed before the earthquake and houses destroyed

The geophysical analysis determined a high correlation between the values of resistivity obtained by the electrical tomography and the conductivity values of the radargrams and the DINSAR methods and the concentration of structural lineaments.

Especially in Zero Zone, the Felipe Navarrete Mall where more than 96 people died, the greatest seismic stress represented the traces of deformation, possibly amplified the Rayleigh surface waves that affected the areas between the Felipe Navarrete Shopping Center, the Banco del Pichincha and the Central Market. This zone continues to be the one with the greatest tectonic deformation and the one with the highest susceptibility to earthquakes such as the one that occurred on April 16, 2016.

The two methods of sinking and subsidence analysis by Interferometry-DINSAR and determination of structural lineations, fractures and deformations obtained by concentration of structural lineaments, are complementary, while the DINSAR model, which needs a lot of calculation time to analyze the rate of change of the topographic gradient in a period of time in small spaces of movement (cm), the density model of concentration of structural lineaments, based on digital models of elevation of high resolution (in this case of 4 m), provides quickly, and at low cost, areas of maximum terrain surface deformation with high precision.

Acknowledgements This research was funded by the project: Junta Castilla y León SA044G18.

References

Antón A, Avilés A (2017) Analysis of seismic response and liquefaction potential in the Tarqui parish, after the 2016 earthquake (undergraduate thesis). Polytechnic School Faculty of Engineering Earth Sciences (ESPOL). Guayaquil-Ecuador. https://www.dspace.espol.edu.ec/retrieve/100333/D-CD70229.pdf

Cando-Jácome M, Martínez-Graña A (2018) Numerical modeling of flow patterns applied to the analysis of the susceptibility to movements of the ground. Geosciences (Switzerland). 8:340. https://doi.org/10.3390/geosciences8090340

Chunga K, Aguiar R, Zambrano S (2018) Characterization of geological faults capable of generating cortical earthquakes in the Gulf of Guayaquil, south coast of Ecuador 2018. http://www.andeangeology.cl/index.php/revista1/article/view/V46n1-2991

EH/AA/JS (2016a) Geophysical Institute National Polytechnic School. SPECIAL SEISMIC REPORTN. 7 2016. https://www.igepn.edu.ec/eq20160416-informes-noticias?start=20. Accessed 17 Apr 2016

EH/AA/SV/MR (2016b) Geophysical Institute National Polytechnic School. Special Seismic Report No. 13 – 2016. Technical report of the Pedernales earthquake. 19h50 TL. https://www.igepn.edu.ec/servicios/noticias/1317-informe-sismico-especial-n-13-2016. Accessed 17 Apr 2016

Gutscher M, Malavieille L, Lallemand J, Collot Y (1999) Tectonic segmentation of the North Andean margin: impact of the Carnegie Ridge collision. Earth Planet Sci Lett 168:255–270. http://www.gm.univ-montp2.fr/spip/IMG/pdf/Gutscher-EPSL99-Andes.pdf

IASR (2016a) Secretary of Risk Management. Informe N° SGR-IASR-08-009. Report of the study of analysis of Differential Radar Interferometry (INSAR) for estimation of soil deformation in the area affected by the earthquake on 04-16-2016. 13-07-2016. Internal document not published

IASR (2016b) Undersecretary of Information Management and Risk Analysis. Report No. SGR-IASR-08-0045-2016. Geophysical prospecting in Zone 0—Tarqui Parish of the Manta, Manabí Province. Internal document not published

Marcaillou B, Collot J-Y, Ribodetti A, d'Acremont E, Mahamat A-A, Alvarado A (2016) Seamount subduction at the North-Ecuadorian convergent margin: Effects on structures, inter-seismic coupling and seismogenesis. Earth Planet Sci Lett 433:146–158. https://doi.org/10.1016/j.epsl.2015. http://adsabs.harvard.edu/abs/2016E%26PSL.433.146M

Martínez-Graña A, Goy JL, Zazio C, Yenes M (2013) Engineering Geology Maps for Planning and Management of Natural Parks: "Las Batuecas-Sierra de Francia" and "Quilamas" (Central Spanish System, Salamanca, Spain). Geosciences 3(1):46–62

Montes RV, Martínez-Graña AM, Martínez Catalán JR, Arribas PA, Sánchez San Román FJ, Zazo C (2017) Integration of GIS, electromagnetic and electrical methods in the delimitation of groundwater polluted by effluent discharge (Salamanca, Spain): a case study. Int J Environ Res Public Health 14:1369

NEC-11 (2011) Ministry of Urban Development and Housing. Ecuadorian Construction Standard NEC-11 Chapter 2 Seismic Hazard and Resistant Earthquake Design Requirements. Executive decree No. 705 April 2011. https://inmobiliariadja.files.wordpress.com/2016/09/nec2011-cap-02-peligro-sismico-y-requisitos-de-disec3b1o-sismo-resistente-021412-vic.pdf

Norton M (2010) Location of oceanic ridges and plate boundaries on the northwestern edge of South America based on a screenshot from NASA World Wind software—outlines taken from Gutscher et al. 1999. https://es.wikipedia.org/wiki/Archivo:Carnegie_Ridge.png

ODEPLAN (2001) Office of Planning of the Presidency (ODEPLAN). Cartography of the threats of natural origin by canton in Ecuador. Preliminary report. 2001. http://horizon.documentation.ird.fr/exl-doc/pleins_textes/divers16-03/010065702.pdf

Toprak S, Holzer T, Bennett M, Tinsley J (1999) CPT-and SPT-based probabilistic assessment of liquefaction potential. https://www.researchgate.net/publication/277343077_CPT-and_SPTbased_probabilistic_assessment_of_liquefaction_potential

Vidal Montes R, Martinez-Graña AM, Martínez Catalán JR, Ayarza Arribas P, Sánchez San Román FJ (2016) Vulnerability to groundwater contamination, SW Salamanca, Spain. J Maps 12(sup 1):147–155. https://doi.org/10.1080/17445647.2016.1172271

Winckel A (1997) Los Paisajes Naturales del Ecuador. The regions and landscapes of Ecuador. Basic Geography of Ecuador, Volume IV, vol 2. Geographic Institute of Ecuador-IGM-ORSTOM-IPGH. 1997. http://www.ecuador.ird.fr/mediateca/las-co-ediciones-en-ecuador/los-paisajes-naturales-del-ecuador-tomo-2